Detecting electric charge with extreme mass ratio inspirals

Chao Zhang (张超)[†] and Yungui Gong (龚云贵)[*]

School of Physics, Huazhong University of Science and Technology, Wuhan, Hubei 430074, China

We consider extreme mass ratio inspirals during which an electrically charged compact object with mass m_p and the charge to mass ratio q inspirals around a Schwarzschild black hole of mass M. Using the Teukolsky and generalized Sasaki-Nakamura formalisms for the gravitational and electromagnetic perturbations around a Schwarzschild black hole, we numerically calculate the energy flux of both gravitational and electromagnetic waves induced by a charged particle moving in circular orbits. With one year observation of these extreme mass ratio inspirals, we show that a space-based gravitational wave detector such as the Laser Interferometer Space Antenna can detect the charge to mass ratio as small as $q \sim 10^{-3}$.

I. INTRODUCTION

The first direct detection of gravitational wave (GW) event GW150914 in 2015 by the Laser Interferometer Gravitational-Wave Observatory (LIGO) Scientific Collaboration and the Virgo Collaboration [1,2] provides us a new window to understand the nature of gravity in the nonlinear and strong field regimes. To date, there have been tens of confirmed GW detections in the frequency range of tens to hundreds Hertz [3–6]. However, due to the seismic noise and gravity gradient noise, the ground-based GW observatories can only measure GWs within the frequency range 10–10^3 Hz, and are unable to explore lower frequency band 10^{-4}–10^{-1} Hz where a wealth of astrophysical signals reside. The proposed space-based observatories like the Laser Interferometer Space Antenna (LISA) [7,8], TianQin [9], and Taiji [10] are expected to detect GWs in this low-frequency regime. Extreme mass ratio inspirals (EMRIs) are among the most promising GW sources expected to be detected for these future space-based GW detectors. An EMRI consists of a stellar mass compact object (secondary object) with mass m_p such as a black hole (BH) or a neutron star orbiting around a supermassive black hole (SMBH) (primary object) of mass M, with the mass ratio m_p/M in the range of 10^{-7}–10^{-4}. The binary emits GWs while the secondary object slowly inspirals into the primary object under the gravitational radiation reaction, so EMRIs provide a unique wealth of information about the masses, spins, electric charges, the strong-field physics in the vicinity of BHs, the astrophysics of their stellar environments, and so on [11–19].

The existence of stable charged astrophysical compact objects in nature remains controversial. Glendening [20] pointed out that macroscopic bodies can have a small amount of charge of approximately 100 Coulombs per solar mass, which does not affect the structure of the star much. In such a system that the star is modeled by a ball of hot ionized gas, the electrons are likely to rise to the top and escape from the star because of the difference in the partial pressure of electrons compared to that of ions. The electric field will be created by the charge separation and then prevent the electrons from escaping further from the star [21]. The electrified star can have positive charge of about 100 Coulombs per solar mass when the equilibrium is reached. However, for highly relativistic stars, the situation might be different when we consider the full effects of general relativity. The highly compact stars, whose radius is on the verge of forming an event horizon, can contain a maximal huge amount of charge with the charge to mass ratio of the order one [22–29]. The huge amount of charge supports the global balance of forces between the matter part and the electrostatic part.

Nevertheless, this balance is unstable and the charged star will collapse to a charged black hole with a perturbation of decrease in the electric field [30]. Charged compact objects can also form through the Wald mechanism where a black hole immersed into a magnetic field selectively accretes charge [31], or by accreting minicharged dark matter beyond the standard model [32]. The electric charge can also play a vital role in halting gravitational collapse through the equilibrium of large bodies [33]. The charged parameter can be applied to construct models of various astrophysical objects of immense gravity by considering the relevant matter distributions. Such models with charged parameter can successfully describe the characteristics of compact stellar objects like neutron stars, quark stars, etc. [34]. Direct observation of electrically charged compact

[*]Corresponding author.
yggong@hust.edu.cn
[†]chao_zhang@hust.edu.cn

bodies would be very challenging, because charged BHs would quickly discharge due to charge dissipation through the presence of the plasma around them or the spontaneous production of electron-positron pairs [35–39]. Nonetheless, EMRIs can be an excellent system for detecting electrically charged compact bodies. The extra emission channel due to electromagnetic radiation accelerates the coalescence, leading to a cumulative dephasing of GWs, which can be distinguished by future space-based GW detectors like LISA, TianQin, and Taiji.

The gravitational and electromagnetic radiations from binary BHs with electric and magnetic charges were studied in [40]. The authors studied the motion of binary BHs with both electric and magnetic charges on circular orbits by combining the Newtonian gravity with the radiation reaction. They found that electric and magnetic charges significantly suppress the merger time of dyonic binaries. The work was later generalized to eccentric orbits and they derived the waveforms for dyonic binary BH inspirals [41]. In [42], the authors took into account astrophysical environments (e.g., accretion disks) in addition to the scalar/vector and gravitational radiations to investigate the eccentricity and orbital evolution for BH binaries, and discussed the competition between radiative mechanisms and environmental effects on the eccentricity evolution. The effect of charged BHs with electromagnetic dipole emission on the estimation of the chirp mass and BH merger were studied in [43,44]. The merger rate distribution of primordial black hole binaries with electric charges and magnetic charges was studies in [45,46]. However, these discussions are mainly based on the Newtonian orbit and dipole emission.

When the secondary object approaches the innermost stable circular orbit (ISCO) of the central BH, the Newtonian approximation breaks down and the above method becomes ill suited in the late phase of inspiral. By solving the full coupled Einstein-Maxwell equations numerically, it was found that GW150914 is consistent with charged BHs with the charge to mass ratio as high as 0.3 [47]. To use the highly relativistic dynamics of EMRIs with charged secondary object to place a more stringent constraint on the possible existed electric charge, we need to get more accurate orbital motion and gravitational waveforms. In this paper, we use the Teukolsky formalism for BH perturbations [48–52] to calculate the orbital evolution of inspiralling into the ISCO. A more detailed presentation of the Teukolsky formalism can be found in [53–56].

The paper is organized as follows. In Sec. II, we introduce the Einstein-Maxwell field equations, the Teukolsky perturbation formalism, and the source terms for the inhomogeneous Teukolsky equations. In Sec. III, we numerically calculate the energy flux for gravitational and electromagnetic fields using the Teukolsky and generalized Sasaki-Nakamura formalisms. In Sec. IV, we give the numerical results of energy flux and use the dephasing

of a GW to constrain the charge to mass ratio. Section V is devoted to conclusions and discussions.

II. EINSTEIN-MAXWELL FIELD EQUATIONS

The Einstein equations and Maxwell equations are

$$G^{\mu\nu} = 8\pi T_p^{\mu\nu} + 8\pi T_e^{\mu\nu}, \tag{1}$$

$$\nabla_\nu F^{\mu\nu} = 4\pi J^\mu, \tag{2}$$

where $G^{\mu\nu}$ is the Einstein tensor, $F_{\mu\nu} = \nabla_\mu A_\nu - \nabla_\nu A_\mu$ is the electromagnetic field tensor, J^μ is the electric 4-current density, and $T_p^{\mu\nu}$ and $T_e^{\mu\nu}$ are the particle's stress-energy tensor and electromagnetic stress-energy tensor, respectively. We consider a charged body with mass m_p and electric charge q per mass (charge to mass ratio) orbiting around a BH of mass M. For an EMRI system with $m_p \ll M$, we can ignore the contribution to the background metric from the electromagnetic field. Since the amplitude of the electromagnetic stress-energy $T_e^{\mu\nu}$ is quadratic in the electromagnetic field, the contribution to the background metric from the electromagnetic field is second order. The perturbed Einstein and Maxwell equations for EMRIs are

$$G^{\mu\nu} = 8\pi T_p^{\mu\nu}, \tag{3}$$

$$\nabla_\nu F^{\mu\nu} = 4\pi J^\mu, \tag{4}$$

where

$$T_p^{\mu\nu}(x) = m_p \int d\tau \, u^\mu u^\nu \delta^{(4)}[x - z(\tau)], \tag{5}$$

$$J^\mu(x) = q m_p \int d\tau \, u^\mu \delta^{(4)}[x - z(\tau)]. \tag{6}$$

We apply the Newman-Penrose formalism [57] to discuss the perturbations induced by a charged particle with mass m_p and electric charge q per mass around a Schwarzschild BH. The metric of Schwarzchild BHs is

$$ds^2 = f(r)dt^2 - \frac{1}{f(r)}dr^2 - r^2 d\Omega^2, \tag{7}$$

where $f(r) = 1–2M/r$. Based on the metric (7), we construct the null tetrad,

$$l^\mu = \left[\frac{r}{r-2M}, 1, 0, 0\right],$$

$$n^\mu = \left[\frac{1}{2}, -\frac{r-2M}{2r}, 0, 0\right],$$

$$m^\mu = \left[0, 0, \frac{1}{\sqrt{2}r}, \frac{i}{\sqrt{2}r\sin\theta}\right],$$

$$\bar{m}^\mu = \left[0, 0, \frac{1}{\sqrt{2}r}, \frac{-i}{\sqrt{2}r\sin\theta}\right]. \tag{8}$$

Then the propagating electromagnetic field is described by the two complex quantities,

$$\phi_0 = F_{\mu\nu}l^\mu m^\nu, \qquad \phi_2 = F_{\mu\nu}\bar{m}^\mu n^\nu. \tag{9}$$

The propagating gravitational field is described by the two complex Newman-Penrose variables

$$\psi_0 = -C_{\alpha\beta\gamma\delta}l^\alpha m^\beta l^\gamma m^\delta,$$
$$\psi_4 = -C_{\alpha\beta\gamma\delta}n^\alpha \bar{m}^\beta n^\gamma \bar{m}^\delta, \tag{10}$$

where $C_{\alpha\beta\gamma\delta}$ is the Weyl tensor. A single master equation for a gravitational perturbation ($s = -2$) and an electromagnetic field ($s = -1$) was derived in Ref. [48],

$$\frac{r^2}{f(r)}\frac{\partial^2\psi}{\partial t^2} - \frac{1}{\sin^2\theta}\frac{\partial^2\psi}{\partial\varphi^2} - \Delta^{-s}\frac{\partial}{\partial r}\left(\Delta^{s+1}\frac{\partial\psi}{\partial r}\right)$$
$$-\frac{1}{\sin\theta}\frac{\partial}{\partial\theta}\left(\sin\theta\frac{\partial\psi}{\partial\theta}\right) - \frac{2is\cos\theta}{\sin^2\theta}\frac{\partial\psi}{\partial\varphi} - 2s$$
$$\times\left[\frac{Mr^2}{\Delta} - r\right]\frac{\partial\psi}{\partial t} + (s^2\cot^2\theta - s)\psi = 4\pi r^2 T, \tag{11}$$

where $\Delta = r^2 - 2Mr$; the explicit field ψ and the corresponding source T are given in Table I [48]. In terms of the spin-weighted spherical harmonics ${}_sY_{lm}(\theta,\varphi)$ [58], the field ψ can be written as

$$\psi = \int d\omega \sum_{l,m} R_{\omega lm}(r)\, {}_sY_{lm}(\theta,\varphi)e^{-i\omega t}, \tag{12}$$

where the radial function $R_{\omega lm}(r)$ satisfies the inhomogeneous Teukolsky equation

TABLE I. The explicit expressions for the field ψ and the corresponding source T.

s	ψ	T
-1	$r^2\phi_2$	$r^2 J_2$
-2	$r^4\psi_4$	$2r^4 T_4$

$$\left(\frac{\omega^2 r^4 - 2is\omega r^2(r-M)}{\Delta} + 4is\omega r - \lambda\right)R_{\omega lm}$$
$$+ \Delta^{-s}\frac{d}{dr}\left(\Delta^{s+1}\frac{dR_{\omega lm}}{dr}\right) = T_{\omega lm}, \tag{13}$$

$\lambda = (l-s)(l+s+1)$, and the source $T_{\omega lm}(r)$ is

$$T_{\omega lm}(r) = \frac{1}{2\pi}\int dt\, d\Omega\, 4\pi r^2 T_s \bar{Y}_{lm}(\theta,\varphi)e^{i\omega t}. \tag{14}$$

For a circular trajectory at r_0 under consideration

$$T_p^{\mu\nu}(x) = \frac{m_p}{r_0^2}\frac{u^\mu u^\nu}{u^t}\delta(r-r_0)\delta(\cos\theta)\delta(\varphi-\Omega t),$$

$$J^\mu(x) = q\frac{m_p}{r_0^2}\frac{u^\mu}{u^t}\delta(r-r_0)\delta(\cos\theta)\delta(\varphi-\Omega t), \tag{15}$$

where

$$u^\mu = (\tilde{E}/f_0, 0, 0, \tilde{L}/r_0^2), \tag{16}$$

the particle's energy per mass $\tilde{E}$, angular momentum per mass $\tilde{L}$, and angular velocity Ω are [53]

$$\tilde{E} = f_0(1 - 3M/r_0)^{-1/2},$$
$$\tilde{L} = (Mr_0)^{1/2}(1 - 3M/r_0)^{-1/2},$$
$$\Omega = (M/r_0^3)^{-1/2}, \tag{17}$$

with $f_0 = 1 - 2M/r_0$. The source term $T_{\omega lm}(r)$ for gravitational perturbation ($s = -2$) was given in [59], while the source term for the electromagnetic field perturbation ($s = -1$) reads

$$T_{\omega lm}(r) = -i\sqrt{2\frac{r}{M}}\pi q\frac{m_p}{M}\left(\frac{r}{M} - 2\right)_{-1}Y_{lm}\left(\frac{\pi}{2}, 0\right)\delta'(r-r_0)\delta(\omega - m\Omega)$$
$$- \pi q\frac{m_p}{M}\left(2 - \frac{r}{M}\right)\sqrt{2l(l+1)}\,_0Y_{lm}\left(\frac{\pi}{2}, 0\right)\delta(r-r_0)\delta(\omega - m\Omega)$$
$$- \frac{\pi q m_p(-2r^2\omega + irM - 2iM^2)}{M^{5/2}\sqrt{2r}}\,_{-1}Y_{lm}\left(\frac{\pi}{2}, 0\right)\delta(r-r_0)\delta(\omega - m\Omega). \tag{18}$$

III. THE NUMERICAL CALCULATION FOR ENERGY FLUX

The homogeneous Teukolsky equation (13) admits two linearly independent solutions $R_{\omega lm}^{\text{in}}$ and $R_{\omega lm}^{\text{up}}$, with the following asymptotic values at the horizon $r = 2M$ and at infinity:

$$R_{\omega lm}^{\text{in}} = \begin{cases} \Delta^{-s} e^{-i\omega r^*}, & (r^* \to -\infty) \\ B^{\text{out}} \frac{e^{i\omega r^*}}{r^{2s+1}} + B^{\text{in}} \frac{e^{-i\omega r^*}}{r}, & (r^* \to +\infty) \end{cases} \quad (19)$$

$$R_{\omega lm}^{\text{up}} = \begin{cases} D^{\text{up}} e^{i\omega r^*} + \frac{D^{\text{in}}}{\Delta^s} e^{-i\omega r^*}, & (r^* \to -\infty) \\ e^{i\omega r^*}, & (r^* \to +\infty) \end{cases} \quad (20)$$

where the tortoise radius $r^* = r + 2M \ln(r/2M - 1)$. The solutions $R_{\omega lm}^{\text{in}}$ and $R_{\omega lm}^{\text{up}}$ are purely outgoing at infinity and purely ingoing at the horizon. With the help of these homogeneous solutions, the solution to Eq. (13) is

$$R_{\omega lm}(r) = \frac{1}{2i\omega B^{\text{in}}} \left(R_{\omega lm}^{\text{in}} \int_{r^*}^{+\infty} \Delta^s R_{\omega lm}^{\text{up}} T_{\omega lm} dr^* \right.$$
$$\left. + R_{\omega lm}^{\text{up}} \int_{-\infty}^{r^*} \Delta^s R_{\omega lm}^{\text{in}} T_{\omega lm} dr^* \right). \quad (21)$$

The energy per unit solid angle carried off by outgoing electromagnetic waves at infinity is

$$\frac{d^2 E_q^\infty}{dt d\Omega} = \lim_{r \to \infty} \frac{r^2}{2\pi} |\phi_2|^2. \quad (22)$$

Since

$$R_{\omega lm}(r \to \infty) = r^2 \phi_2 = q Z_{\omega lm}^\infty \delta(\omega - m\Omega) r e^{i\omega r^*}, \quad (23)$$

so the expression for the energy flux of electromagnetic waves is

$$dE_q^\infty/dt = \dot{E}_q^\infty = q^2 \left(\frac{m_p}{M}\right)^2 \sum_{l=1}^\infty \sum_{m=1}^l \frac{|Z_{\omega lm}^\infty|^2}{\pi}, \quad (24)$$

where

$$Z_{\omega lm}^\infty = \frac{1}{2i\omega q B^{\text{in}}} \int_{2M}^\infty dr' \frac{R^{\text{in}} T_{\omega lm}(r)}{\Delta}$$
$$= \frac{1}{2i\omega B^{\text{in}}} \left\{ \frac{i\sqrt{2}\pi_{-1} Y_{lm}(\frac{\pi}{2}, 0)}{\sqrt{r/M}} \frac{dR_{\omega lm}^{\text{in}}}{dr} \right.$$
$$+ \sqrt{2}\pi R_{\omega lm}^{\text{in}} \left(\frac{\sqrt{l(l+1)}}{r/M} {}_0 Y_{lm}\left(\frac{\pi}{2}, 0\right) \right)$$
$$\left. + \frac{(r^2\omega - iMr + 2iM^2)}{M^{-1/2}(r - 2M)r^{3/2}} {}_{-1} Y_{lm}\left(\frac{\pi}{2}, 0\right) \right) \right\}. \quad (25)$$

The energy carried off by ingoing electromagnetic waves at the horizon is

$$dE_q^H/dt = \dot{E}_q^H = q^2 \left(\frac{m_p}{M}\right)^2 \sum_{l=1}^\infty \sum_{m=1}^l \frac{|Z_{\omega lm}^H|^2}{\pi}, \quad (26)$$

where

$$Z_{\omega lm}^H = \frac{1}{2i\omega B^{\text{in}}} \left\{ \frac{i\sqrt{2}\pi_{-1} Y_{lm}(\frac{\pi}{2}, 0)}{\sqrt{r/M}} \frac{dR_{\omega lm}^{\text{up}}}{dr} \right.$$
$$+ \sqrt{2}\pi R_{\omega lm}^{\text{up}} \left(\frac{\sqrt{l(l+1)}}{r/M} {}_0 Y_{lm}\left(\frac{\pi}{2}, 0\right) \right.$$
$$\left. + \frac{(r^2\omega - iMr + 2iM^2)}{M^{-1/2}(r - 2M)r^{3/2}} {}_{-1} Y_{lm}\left(\frac{\pi}{2}, 0\right) \right) \right\}. \quad (27)$$

The total energy flux emitted by electromagnetic fields is

$$\dot{E}_q = \dot{E}_q^\infty + \dot{E}_q^H. \quad (28)$$

The total energy flux emitted by tensor fields is

$$\dot{E}_t = \dot{E}_t^\infty + \dot{E}_t^H, \quad (29)$$

where the formula for $\dot{E}_t^{\infty,H}$ is given in Refs. [53,56].

The generalized Regge-Wheeler equation is

$$\left[\frac{d^2}{dr^{*2}} + \omega^2 - V_{\text{RW}}(r, s) \right] X_{\omega lm} = 0, \quad (30)$$

where

$$V_{\text{RW}}(r, s) = f(r) \left[\frac{l(l+1)}{r^2} - \frac{2(s^2 - 1)}{r^3} \right]. \quad (31)$$

The homogeneous Regge-Wheeler equation (30) admits two linearly independent solutions $X_{\omega lm}^{\text{in}}$ and $X_{\omega lm}^{\text{up}}$ which are implemented in the *Mathematica* packages of the BH Perturbation Toolkit [60], with the following asymptotic values at the horizon $r = 2M$ and at infinity,

$$X_{\omega lm}^{\text{in}} = \begin{cases} e^{-i\omega r^*} & (r^* \to -\infty) \\ A^{\text{out}} e^{i\omega r^*} + A^{\text{in}} e^{-i\omega r^*} & (r^* \to +\infty) \end{cases}, \quad (32)$$

$$X_{\omega lm}^{\text{up}} = \begin{cases} C^{\text{up}} e^{i\omega r^*} + C^{\text{in}} e^{-i\omega r^*} & (r^* \to -\infty) \\ e^{i\omega r^*} & (r^* \to +\infty) \end{cases}. \quad (33)$$

The solutions $X_{\omega lm}^{\text{in}}$ and $X_{\omega lm}^{\text{up}}$ are purely outgoing at infinity and purely ingoing at the horizon. The Wronskian of $X_{\omega lm}^{\text{in}}$ and $X_{\omega lm}^{\text{up}}$ is

$$W = X_{\omega lm}^{\text{in}} \frac{dX_{\omega lm}^{\text{up}}}{dr^*} - X_{\omega lm}^{\text{up}} \frac{dX_{\omega lm}^{\text{in}}}{dr^*} = 2i\omega A^{\text{in}}. \quad (34)$$

The relation between B^{in} and A^{in} for $s = -2$ is given in [53], while for $s = -1$

$$B^{\text{in}} = \frac{-l(l+1)A^{\text{in}}}{2i\omega}. \tag{35}$$

With the solutions $X^{\text{in,up}}_{\omega lm}$, we can obtain $R^{\text{in,up}}_{\omega lm}$ as follows [61]:

$$R^{\text{in,up}}_{\omega lm} = \left(\frac{\Delta}{r}\right)^{|s|} \mathcal{L}^{|s|} \left[\left(\frac{r}{\sqrt{\Delta}}\right)^{|s|} \frac{X^{\text{in,up}}_{\omega lm}}{r\sqrt{\Delta^s}}\right], \tag{36}$$

where $\mathcal{L} = d/dr + i\omega/f(r)$.

IV. RESULTS

From Eqs. (24) and (26), the energy flux $\dot{E}_q$ emitted by the electromagnetic field is proportional to the squared mass ratio $(m_p/M)^2$ and squared electric charge q^2. Figure 1 shows the normalized flux $m_p^{-2}M^2\dot{E}_q$ which depends only on the dimensionless electric charge q (the charge to mass ratio). The emission power due to electromagnetic radiation increases as the orbital velocity $v = (M\Omega)^{1/3}$ increases while the particle inspiraling toward the ISCO at $r = 6M$. The extra emission channel due to electromagnetic radiation accelerates the coalescence, leaving a significant imprint on gravitational waves. From Fig. 1, we see that the behavior of the electromagnetic flux in the case of slow motion with the velocity $v \ll 1$ is consistent with the result of electromagnetic dipole radiation for a Newtonian binary [40,42,46]

$$\dot{E}_q^{\text{Newtonian}} = \frac{2q^2m_p^2M^2}{3r^4} = \frac{2q^2m_p^2}{3M^2}v^8. \tag{37}$$
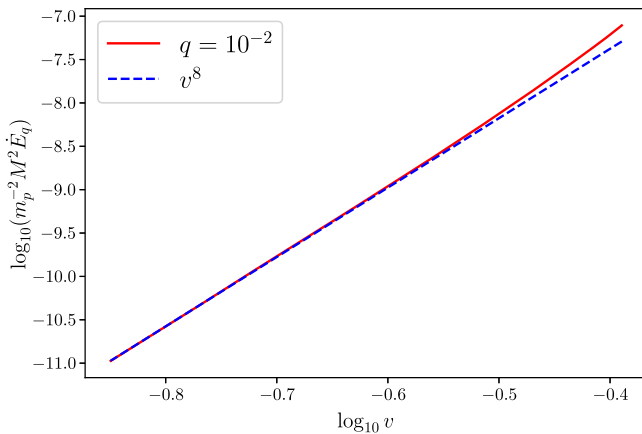

FIG. 1.   The radiation power from a charged particle with the charge to mass ratio $q = 10^{-2}$ as a function of the orbital speed $v = (M\Omega)^{1/3}$. The blue dashed line represents the emission power v^8 due to electromagnetic dipole radiation in a Newtonian binary or flat spacetime background.

Far away from the central BH, the speed of the particle is much less than the speed of light, and the main electromagnetic radiation is the electric dipole radiation with the radiated power falling off as v^8. In the strong field regions near ISCO, the emission power of electromagnetic waves differs from v^8; this can be interpreted as the interaction between the electromagnetic filed and the gravitational field. To compare electromagnetic and gravitational radiation, we show the ratio $\dot{E}_q/\dot{E}_t$ as a function of the orbital speed v in Fig. 2. The ratio decreases as the orbital speed increases, since the emission power $\dot{E}_t$ of gravitational waves grows as v^{10} [55], so it grows faster than that of electromagnetic waves with v^8 on the assumption that the weak field limit is still applicable. As expected in Fig. 2, the contribution of electromagnetic waves becomes larger if the particle has more charge.

To detect the electric charge of the small compact object (particle) in the EMRI, we compare the number of cycles between charged and uncharged particles accumulated before the merger [62],

$$\mathcal{N} = \int_{f_{\min}}^{f_{\max}} \frac{f_{\text{GW}}}{\dot{f}_{\text{GW}}} df_{\text{GW}}, \tag{38}$$

where the GW frequency $f_{\text{GW}} = 2\Omega$,

$$\dot{f}_{\text{GW}} = \frac{3}{2} \frac{f_{\text{GW}}}{r_0} \frac{dr}{d\tilde{E}}\bigg|_{r_0} \dot{E}, \tag{39}$$

and $\tilde{E}$ is the particle's orbital energy per mass. We choose $f_{\max} = (6^{3/2}\pi M)^{-1}$ and $f_{\min} = \max[f_T, 10^{-4}]$, where f_T is the GW frequency one year before the ISCO [63] and the cutoff frequency for LISA is 10^{-4} [64]. In the Newtonian approximation, $\tilde{E} = -M/(2r)$, Eq. (39) reduces to the major semiaxis evolution in [42],
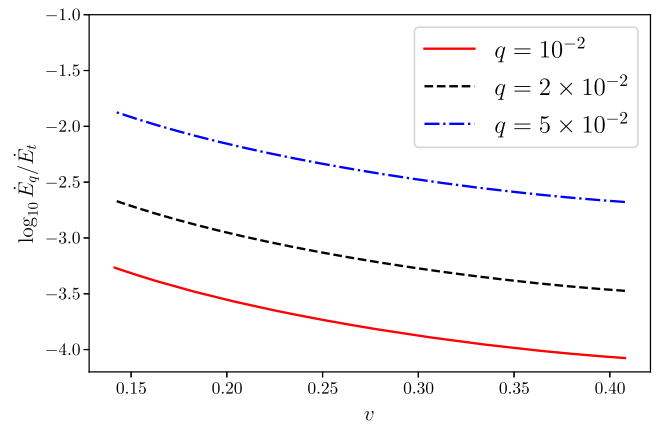

FIG. 2.   The relative difference between the GW flux and the electromagnetic flux as a function of the orbital speed $v = (M\Omega)^{1/3}$ for a charged particle with different charge to mass ratio q.
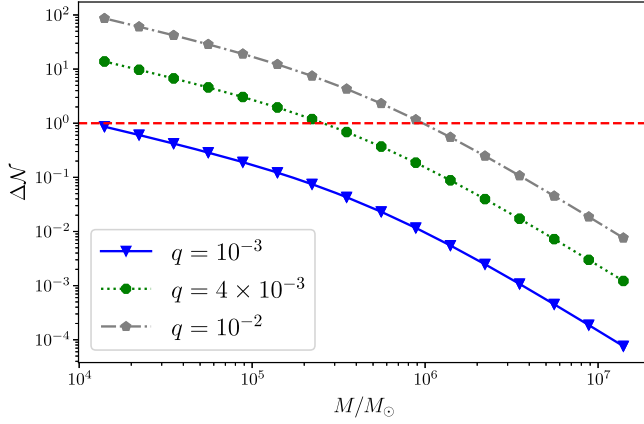
FIG. 3. The difference in the number of GW cycles accumulated by EMRIs on a circular orbit. The mass of the charged particle is fixed to be $m_p = 1.4 \; M_\odot$, the mass of the central black hole varies in the range $M \in [1.4 \times 10^4, 1.4 \times 10^7] \; M_\odot$, and the charge to mass ratio q is chosen as $q = 10^{-3}$ (blue solid line), $q = 4 \times 10^{-3}$ (green dotted line), $q = 10^{-2}$ (gray dash-dotted line), respectively. The red dashed line corresponds to the threshold above which the two signals are distinguished by LISA. All binaries are observed one year before merger.

$$\dot{r} = -\frac{2r^2}{Mm_p}\dot{E}. \tag{40}$$

Now we fix the particle's mass to be $m_p = 1.4 \; M_\odot$, but vary its charge q and choose different mass $M \in [1.4 \times 10^4, 1.4 \times 10^7] \; M_\odot$ for the central black hole to calculate $\Delta\mathcal{N} = \mathcal{N}(q = 0) - \mathcal{N}(q)$ and the result is shown in Fig. 3. As discussed above, the extra emission channel due to electromagnetic radiation accelerates the coalescence, so for the same one year observation before the merger, the charged particle starts further away from ISCO and the difference $\Delta\mathcal{N}$ is always positive. As shown in Fig. 3, $\Delta\mathcal{N}$ increases monotonically as the charge to mass ratio q becomes bigger, and it strongly depends on the mass of the central BH such that lighter BHs have larger $\Delta\mathcal{N}$. For lighter BHs, the orbital speed v of the charged particle is smaller at the beginning that is one year prior to the ISCO, so the contribution of electromagnetic fluxes is larger as shown in Fig. 2. Henceforth the dephasing is bigger,

leading to larger $\Delta\mathcal{N}$ for a one-year observation. Following Ref. [65], we take the threshold for a detectable dephasing that two signals are distinguished by LISA as 1 radian. From Fig. 3, we see that the dephasing $\Delta\mathcal{N}$ can be larger than 1 radian for $M \sim 10^4 \; M_\odot$ and $q \geq 10^{-3}$ with one year's observation before merger. Therefore LISA can detect the charge to mass ratio $q \sim 10^{-3}$ with one year observation of EMRIs.

V. CONCLUSIONS

We study the energy emissions and GWs from EMRIs with a small charged compact object with mass m_p and the charge to mass ratio q inspiralling into a SMBH. We derive the source term $T_{\omega lm}$ for solving the inhomogeneous Teukolsky equation with an electromagnetic field, and calculate the total emission power due to both gravitational and electromagnetic radiations. Compared with the power emitted by electromagnetic field from the circular orbit in a flat background as shown in Fig. 1, the emission power in a strong gravitational field is bigger for the reason of the coupling between gravitational and electromagnetic fields. We also discuss the ratio $\dot{E}_q/\dot{E}_t$ as a function of the orbital speed v, and we find that the gravitational radiation $\dot{E}_t$ grows faster than the electromagnetic field contribution $\dot{E}_q$ as the orbital speed v increases. By using the difference of number of cycles $\Delta\mathcal{N}$ accumulated before the merger between a charged particle with the charge to mass ratio q and a neutral particle, we demonstrate that LISA can detect the charge to mass ratio of the small compact object in an EMRI on circular orbits as small as 10^{-3}. Our method of calculation can be straightforwardly extended to generic orbits around Kerr BHs.

ACKNOWLEDGMENTS

[1] B. P. Abbott *et al.* (LIGO Scientific and VIRGO Collaborations), Observation of Gravitational Waves from a Binary Black Hole Merger, Phys. Rev. Lett. **116**, 061102 (2016).

[2] B. P. Abbott *et al.* (LIGO Scientific and VIRGO Collaborations), GW150914: The Advanced LIGO Detectors in the Era of First Discoveries, Phys. Rev. Lett. **116**, 131103 (2016).

[3] B. P. Abbott *et al.* (LIGO Scientific and VIRGO Collaborations), GWTC-1: A Gravitational-Wave Transient Catalog of Compact Binary Mergers Observed by LIGO and Virgo During the First and Second Observing Runs, Phys. Rev. X **9**, 031040 (2019).

[4] R. Abbott *et al.* (LIGO Scientific and VIRGO Collaborations), GWTC-2: Compact Binary Coalescences Observed

by LIGO and Virgo During the First Half of the Third Observing Run, Phys. Rev. X **11,** 021053 (2021).

[5] R. Abbott *et al.* (LIGO Scientific and VIRGO Collaborations), GWTC-2.1: Deep extended catalog of compact binary coalescences observed by LIGO and Virgo during the first half of the third observing run, arXiv:2108.01045.

[6] R. Abbott *et al.* (LIGO Scientific, VIRGO and KAGRA Collaborations), GWTC-3: Compact binary coalescences observed by LIGO and Virgo during the second part of the third observing run, arXiv:2111.03606.

[7] K. Danzmann, LISA: An ESA cornerstone mission for a gravitational wave observatory, Classical Quantum Gravity **14,** 1399 (1997).

[8] P. Amaro-Seoane *et al.* (LISA Collaboration), Laser interferometer space antenna, arXiv:1702.00786.

[9] J. Luo *et al.* (TianQin Collaboration), TianQin: A space-borne gravitational wave detector, Classical Quantum Gravity **33,** 035010 (2016).

[10] W.-R. Hu and Y.-L. Wu, The Taiji Program in Space for gravitational wave physics and the nature of gravity, Natl. Sci. Rev. **4,** 685 (2017).

[11] P. Amaro-Seoane, J. R. Gair, M. Freitag, M. Coleman Miller, I. Mandel, C. J. Cutler, and S. Babak, Astrophysics, detection and science applications of intermediate- and extreme mass-ratio inspirals, Classical Quantum Gravity **24,** R113 (2007).

[12] S. Babak, J. Gair, A. Sesana, E. Barausse, C. F. Sopuerta, C. P. L. Berry, E. Berti, P. Amaro-Seoane, A. Petiteau, and A. Klein, Science with the space-based interferometer LISA. V: Extreme mass-ratio inspirals, Phys. Rev. D **95,** 103012 (2017).

[13] C. P. L. Berry, S. A. Hughes, C. F. Sopuerta, A. J. K. Chua, A. Heffernan, K. Holley-Bockelmann, D. P. Mihaylov, M. C. Miller, and A. Sesana, The unique potential of extreme mass-ratio inspirals for gravitational-wave astronomy, arXiv: 1903.03686.

[14] H.-M. Fan, Y.-M. Hu, E. Barausse, A. Sesana, J.-d. Zhang, X. Zhang, T.-G. Zi, and J. Mei, Science with the TianQin observatory: Preliminary result on extreme-mass-ratio inspirals, Phys. Rev. D **102,** 063016 (2020).

[15] T.-G. Zi, J.-D. Zhang, H.-M. Fan, X.-T. Zhang, Y.-M. Hu, C. Shi, and J. Mei, Science with the TianQin observatory: Preliminary results on testing the no-hair theorem with extreme mass ratio inspirals, Phys. Rev. D **104,** 064008 (2021).

[16] K. Destounis, A. G. Suvorov, and K. D. Kokkotas, Testing spacetime symmetry through gravitational waves from extreme-mass-ratio inspirals, Phys. Rev. D **102,** 064041 (2020).

[17] K. Destounis, A. G. Suvorov, and K. D. Kokkotas, Gravitational-Wave Glitches in Chaotic Extreme-Mass-Ratio Inspirals, Phys. Rev. Lett. **126,** 141102 (2021).

[18] K. Destounis and K. D. Kokkotas, Gravitational-wave glitches: Resonant islands and frequency jumps in non-integrable extreme-mass-ratio inspirals, Phys. Rev. D **104,** 064023 (2021).

[19] V. Cardoso, K. Destounis, F. Duque, R. P. Macedo, and A. Maselli, Black holes in galaxies: Environmental impact on gravitational-wave generation and propagation, Phys. Rev. D **105,** L061501 (2022).

[20] N. Glendenning, *Compact Stars: Nuclear Physics, Particle Physics and General Relativity*, 2nd ed. (Springer, New York, 2000).

[21] J. Bally and E. R. Harrison, The electrically polarized universe, Astrophys. J. **220,** 743 (1978).

[22] J. D. Bekenstein, Hydrostatic equilibrium and gravitational collapse of relativistic charged fluid balls, Phys. Rev. D **4,** 2185 (1971).

[23] F. de Felice, Y. Yu, and J. Fang, Relativistic charged spheres, Mon. Not. R. Astron. Soc. **277,** L17 (1995).

[24] F. de Felice, S.-m. Liu, and Y.-q. Yu, Relativistic charged spheres. 2. Regularity and stability, Classical Quantum Gravity **16,** 2669 (1999).

[25] B. V. Ivanov, Static charged perfect fluid spheres in general relativity, Phys. Rev. D **65,** 104001 (2002).

[26] S. D. Majumdar, A class of exact solutions of Einstein's field equations, Phys. Rev. **72,** 390 (1947).

[27] J. L. Zhang, W. Y. Chau, and T. Y. Deng, The influence of a net charge on the critical mass of a neutron star, Astrophys. Space Sci. **88,** 81 (1982).

[28] P. Anninos and T. Rothman, Instability of extremal relativistic charged spheres, Phys. Rev. D **65,** 024003 (2001).

[29] W. B. Bonnor and S. B. P. Wickramasuriya, Are very large gravitational redshifts possible, Mon. Not. R. Astron. Soc. **170,** 643 (1975).

[30] S. Ray, A. L. Espindola, M. Malheiro, J. P. S. Lemos, and V. T. Zanchin, Electrically charged compact stars and formation of charged black holes, Phys. Rev. D **68,** 084004 (2003).

[31] R. M. Wald, Black hole in a uniform magnetic field, Phys. Rev. D **10,** 1680 (1974).

[32] V. Cardoso, C. F. B. Macedo, P. Pani, and V. Ferrari, Black holes and gravitational waves in models of minicharged dark matter, J. Cosmol. Astropart. Phys. 05 (2016) 054; Erratum, J. Cosmol. Astropart. Phys. 04 (2020) 01.

[33] W. B. Bonnor, The equilibrium of a charged sphere, Mon. Not. R. Astron. Soc. **129,** 443 (1965).

[34] P. M. Takisa, S. Ray, and S. D. Maharaj, Charged compact objects in the linear regime, Astrophys. Space Sci. **350,** 733 (2014).

[35] G. W. Gibbons, Vacuum polarization and the spontaneous loss of charge by black holes, Commun. Math. Phys. **44,** 245 (1975).

[36] D. M. Eardley and W. H. Press, Astrophysical processes near black holes, Annu. Rev. Astron. Astrophys. **13,** 381 (1975).

[37] R. S. Hanni, Limits on the charge of a collapsed object, Phys. Rev. D **25,** 2509 (1982).

[38] P. S. Joshi and J. V. Narlikar, Limits of the charge of a collapsed object, Pramana **18,** 385 (1982).

[39] Y. Gong, Z. Cao, H. Gao, and B. Zhang, On neutralization of charged black holes, Mon. Not. R. Astron. Soc. **488,** 2722 (2019).

[40] L. Liu, O. Christiansen, Z.-K. Guo, R.-G. Cai, and S. P. Kim, Gravitational and electromagnetic radiation from binary black holes with electric and magnetic charges: Circular orbits on a cone, Phys. Rev. D **102,** 103520 (2020).

[41] L. Liu, O. Christiansen, W.-H. Ruan, Z.-K. Guo, R.-G. Cai, and S. P. Kim, Gravitational and electromagnetic radiation

from binary black holes with electric and magnetic charges: Elliptical orbits on a cone, Eur. Phys. J. C **81,** 1048 (2021).

[42] V. Cardoso, C. F. B. Macedo, and R. Vicente, Eccentricity evolution of compact binaries and applications to gravitational-wave physics, Phys. Rev. D **103,** 023015 (2021).

[43] O. Christiansen, J. Beltrán Jiménez, and D. F. Mota, Charged black hole mergers: Orbit circularisation and chirp mass bias, Classical Quantum Gravity **38,** 075017 (2021).

[44] P. Jai-akson, A. Chatrabhuti, O. Evnin, and L. Lehner, Black hole merger estimates in Einstein-Maxwell and Einstein-Maxwell-dilaton gravity, Phys. Rev. D **96,** 044031 (2017).

[45] L. Liu and S. P. Kim, Merger rate of charged black holes from the two-body dynamical capture, J. Cosmol. Astropart. Phys. 03 (2022) 059.

[46] L. Liu, Z.-K. Guo, R.-G. Cai, and S. P. Kim, Merger rate distribution of primordial black hole binaries with electric charges, Phys. Rev. D **102,** 043508 (2020).

[47] G. Bozzola and V. Paschalidis, General Relativistic Simulations of the Quasicircular Inspiral and Merger of Charged Black Holes: GW150914 and Fundamental Physics Implications, Phys. Rev. Lett. **126,** 041103 (2021).

[48] S. A. Teukolsky, Perturbations of a rotating black hole. 1. Fundamental equations for gravitational electromagnetic and neutrino field perturbations, Astrophys. J. **185,** 635 (1973).

[49] W. H. Press and S. A. Teukolsky, Perturbations of a rotating black hole. II. Dynamical stability of the Kerr metric, Astrophys. J. **185,** 649 (1973).

[50] S. A. Teukolsky and W. H. Press, Perturbations of a rotating black hole. III—Interaction of the hole with gravitational and electromagnetic radiation, Astrophys. J. **193,** 443 (1974).

[51] F. J. Zerilli, Effective Potential for Even Parity Regge-Wheeler Gravitational Perturbation Equations, Phys. Rev. Lett. **24,** 737 (1970).

[52] S. Chandrasekhar, On the equations governing the perturbations of the Schwarzschild black hole, Proc. R. Soc. A **343,** 289 (1975).

[53] E. Poisson, Gravitational radiation from a particle in circular orbit around a black hole. 1: Analytical results for the nonrotating case, Phys. Rev. D **47,** 1497 (1993).

[54] E. Poisson, Gravitational radiation from a particle in circular orbit around a black hole. 6. Accuracy of the post-Newtonian expansion, Phys. Rev. D **52,** 5719 (1995); **55,** 7980(A) (1997).

[55] T. Apostolatos, D. Kennefick, E. Poisson, and A. Ori, Gravitational radiation from a particle in circular orbit around a black hole. 3: Stability of circular orbits under radiation reaction, Phys. Rev. D **47,** 5376 (1993).

[56] C. Cutler, D. Kennefick, and E. Poisson, Gravitational radiation reaction for bound motion around a Schwarzschild black hole, Phys. Rev. D **50,** 3816 (1994).

[57] E. T. Newman and R. Penrose, Note on the Bondi-Metzner-Sachs group, J. Math. Phys. (N.Y.) **7,** 863 (1966).

[58] J. N. Goldberg, A. J. MacFarlane, E. T. Newman, F. Rohrlich, and E. C. G. Sudarshan, Spin s spherical harmonics and edth, J. Math. Phys. (N.Y.) **8,** 2155 (1967).

[59] M. Sasaki and T. Nakamura, The regge-wheeler equation with sources for both even and odd parity perturbations of the schwarzschild geometry, Phys. Lett. **87A,** 85 (1981).

[60] Black Hole Perturbation Toolkit, bhptoolkit.org.

[61] S. A. Hughes, Computing radiation from Kerr black holes: Generalization of the Sasaki-Nakamura equation, Phys. Rev. D **62,** 044029 (2000); Erratum, Phys. Rev. D **67,** 089902 (2003).

[62] E. Berti, A. Buonanno, and C. M. Will, Estimating spinning binary parameters and testing alternative theories of gravity with LISA, Phys. Rev. D **71,** 084025 (2005).

[63] P. Pani, V. Cardoso, and L. Gualtieri, Gravitational waves from extreme mass-ratio inspirals in Dynamical Chern-Simons gravity, Phys. Rev. D **83,** 104048 (2011).

[64] P. Amaro-Seoane et al. (LISA Collaboration), Laser interferometer space antenna, arXiv:1702.00786.

[65] A. Maselli, N. Franchini, L. Gualtieri, and T. P. Sotiriou, Detecting Scalar Fields with Extreme Mass Ratio Inspirals, Phys. Rev. Lett. **125,** 141101 (2020).